Modeling of octave-spanning Kerr frequency combs using a generalized mean-field Lugiato–Lefever model

Stéphane Coen,[1,*] Hamish G. Randle,[1] Thibaut Sylvestre,[2] and Miro Erkintalo[1]

[1]*Physics Department, The University of Auckland, Private Bag 92019, Auckland 1142, New Zealand*

[2]*Institut FEMTO-ST, Département d'Optique P. M. Duffieux, Université de Franche-Comté, CNRS, Besançon 25000, France*

**Corresponding author: s.coen@auckland.ac.nz*

Received October 31, 2012; accepted November 20, 2012;
posted December 4, 2012 (Doc. ID 179025); published December 21, 2012

A generalized Lugiato–Lefever equation is numerically solved with a Newton–Raphson method to model Kerr frequency combs. We obtain excellent agreement with past experiments, even for an octave-spanning comb. Simulations are much faster than with any other technique despite including more modes than ever before. Our study reveals that Kerr combs are associated with temporal cavity solitons and dispersive waves, and opens up new avenues for the understanding of Kerr-comb formation.

OCIS codes: 230.5750, 190.5530, 190.4380.

First observed in 2007, frequency-comb generation in monolithic microring resonators has aroused significant research interest [1,2]. A minuscule footprint, power efficiency, and CMOS compatibility make said structures ideal for on-chip frequency-comb generation. Applications range from spectroscopy to telecommunications.

Although comb generation in high-Q Kerr resonators has been extensively reported experimentally, theoretical studies are comparatively scarce. In part this deficiency can be linked to the intractable computational complexity of the existing models. Indeed, the use of a nonlinear Schrödinger (NLS) equation and appropriate coupling-mediated boundary conditions requires hundreds of millions of roundtrips for convergence, owing to the exceedingly high Q of the structures [3]. Likewise the number of four-wave-mixing-mediated coupling terms in coupled-mode equation models scales cubically with the number of modes, limiting such modeling to narrowband combs [4]. Matsko *et al.* [5] also considered an analytic approach, but it is restricted to resonators of infinite intrinsic Q factor and with group-velocity dispersion (GVD) limited to second order. Clearly, a growing demand exists for realistic yet computationally efficient methods for the modeling of frequency combs in high-Q resonators.

In this Letter, we report on direct numerical modeling of Kerr frequency combs using a generalized Lugiato–Lefever (LL) equation [6], and find good agreement with reported experiments. Significantly, the conducted computations are far less intensive than previous methods, allowing for the rapid modeling of octave-spanning combs with arbitrarily low repetition rates on a consumer-grade computer. We also show that the results obtained from the proposed model provide significant insights into Kerr combs. In particular, we highlight how localized dissipative structures known as temporal cavity solitons (CSs) [7] are stable stationary solutions of the governing equation, and how specific comb features can be intuitively described in terms of CS propagation. We expect the reported technique to become an invaluable tool for the understanding and tailoring of nonlinear optical phenomena in high-Q resonators.

We consider a typical ring-resonator configuration (Fig. 1): a continuous-wave (cw) driving field E_{in} with power $P_{\mathrm{in}} = |E_{\mathrm{in}}|^2$ is coherently added to the lightwave circulating in the resonator through a coupler with power transmission coefficient θ. The fourth port of the coupler is used to extract the output field. Mathematically the intracavity field $E^{(m+1)}(0,\tau)$ at the beginning of the $(m+1)$th roundtrip can be related to the field $E^{(m)}(L,\tau)$ at the end of the mth roundtrip as

$$E^{(m+1)}(0,\tau) = \sqrt{\theta}E_{\mathrm{in}} + \sqrt{1-\theta}E^{(m)}(L,\tau)e^{i\phi_0}, \quad (1)$$

where τ is the time, L the is roundtrip length of the resonator, and ϕ_0 the linear phase accumulated by the intracavity field with respect to the pump field over one roundtrip.

Assuming that light propagates in a single spatial mode, the evolution of the field through one roundtrip of the resonator is governed by the well-known (generalized) NLS equation:

$$\frac{\partial E(z,\tau)}{\partial z} = -\frac{\alpha_{\mathrm{i}}}{2}E + i\sum_{k\geq 2}\frac{\beta_k}{k!}\left(i\frac{\partial}{\partial\tau}\right)^k E + i\gamma|E|^2E. \quad (2)$$

Here α_{i} is the linear absorption coefficient inside the resonator, $\beta_k = d^k\beta/d\omega^k|_{\omega=\omega_0}$ are the dispersion coefficients associated with the Taylor series expansion of the propagation constant $\beta(\omega)$ about the center frequency ω_0 of the driving field, and $\gamma = n_2\omega_0/(cA_{\mathrm{eff}})$ is the nonlinearity coefficient with n_2 the nonlinear refractive index and A_{eff} the effective modal area of the resonator mode.

The boundary conditions in Eq. (1) combined with the NLS Eq. (2) form an infinite-dimensional map that describes completely the dynamics of a ring resonator of any size or shape (toroid, racetrack, etc.). In low-loss structures, the field varies only slightly between consecutive

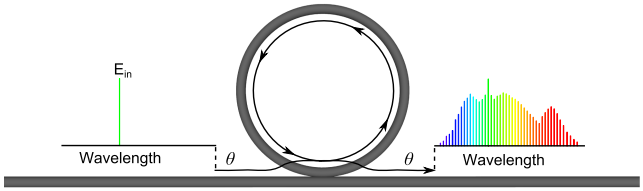

Fig. 1. (Color online) Schematic of the resonator configuration.

roundtrips, making direct simulations of these equations very slow [3]. In these conditions, however, it is well known that Eqs. (1) and (2) can be averaged into an externally driven NLS equation (see, e.g., [8]),

$$t_R \frac{\partial E(t,\tau)}{\partial t} = \left[-\alpha - i\delta_0 + iL\sum_{k\geq 2} \frac{\beta_k}{k!}\left(i\frac{\partial}{\partial \tau}\right)^k + i\gamma L|E|^2 \right] E + \sqrt{\theta} E_{\text{in}}, \tag{3}$$

where t_R is the roundtrip time, $\alpha = (\alpha_i + \theta)/2$ describes the total cavity losses, and $\delta_0 = 2\pi l - \phi_0$ is the detuning with l the order of the cavity resonance closest to the driving field. The continuous variable t measures the *slow time* of the cavity, and can be linked to the roundtrip index as $E(t = mt_R, \tau) = E^{(m)}(0, \tau)$. Equation (3) coincides with the master equation of [5] and, with $\beta_k = 0$ for $k \geq 3$, is formally identical to the mean-field LL model of a diffractive cavity [6,9,10]. It has also been extensively used for the description of passive cavities constructed of single-mode fibers [7,8,11,12]. In particular, spatial pattern formation and the so-called modulation instability (MI) studied in some of these earlier works can be directly connected to frequency-comb generation [6,9,12]. MI was also shown to occur in the normal GVD regime in presence of cavity boundary conditions [8,11], which is directly relevant to combs. We must also note that the expressions of the characteristic bistable response of the LL model as well as those of the intracavity MI gain [8] in fact coincide after normalization with corresponding results obtained from the coupled-mode equations of [4], suggesting an intrinsic link between the two approaches.

The generalized LL Eq. (3) holds in the limit of high-finesse cavities $\mathcal{F} \gg 1$. For typical high-Q resonators, the finesse $\mathcal{F} \sim 10^2$–10^5. Also, dispersion must be "weak" over one roundtrip, $\sum_{k\geq 2} \beta_k L \Delta\omega^k/k! \lesssim \pi$, where $\Delta\omega$ is the (angular) spectral width of the generated comb. This condition was found to be satisfied *a posteriori* for all the results discussed below, thereby asserting the validity of Eq. (3) for the description of Kerr combs. The LL equation has two substantial advantages compared to the infinite-dimensional map Eqs. (1) and (2). On the one hand, Eq. (3) can be numerically integrated with the split-step Fourier method using an integration step corresponding to *multiple roundtrips*, significantly reducing the computational burden in obtaining steady-state solutions. On the other hand, the steady-state solutions can be obtained directly by setting $\partial E/\partial t = 0$ and looking for the roots of the right-hand side of Eq. (3). Although the latter approach does not yield insights into the dynamics of comb formation, it is computationally orders of magnitude more efficient than split-step integration. Here we restrict our attention to stationary solutions obtained by a multidimensional root-finding Newton–Rhapson method. Derivatives are computed with Fourier transforms and the span of the temporal window coincides with t_R, meaning the samples of our frequency grid are spaced by the free spectral range, FSR $= 1/t_R$.

As a first example, we plot in Fig. 2(a) the *intracavity* spectrum of a stable steady-state solution of Eq. (3) obtained with simulation parameters listed in the caption and approximating the experimental values of [13]. We note that some of these parameters have large uncertainties, but this does not invalidate our conclusions. Figure 2(b) is the corresponding experimental *output* spectrum, and clearly excellent agreement is observed (abstraction must be made of the pump-mode intensity, which is modified at the output by the reflected pump). Some of the discrepancies could be traced to effects unaccounted for in Eq. (3), such as wavelength-dependent losses or overlap integrals, or to experimental fluctuations. We also show the temporal profile of the solution as an inset of Fig. 2(a) so as to highlight that the intracavity field corresponds to a ~400 fs duration pulse with a peak power of 100 mW atop a weak cw background. It is well known that the LL equation possesses such localized-CS solutions repeating at the cavity repetition rate, thus forming a frequency comb in the spectral domain [7,10]. In fact, in solving Eq. (3), we have not found any type of stable steady-state comb solutions not made up of single or multiple CSs. This strongly suggests that stable frequency combs generated in high-Q cavities generally correspond to trains of CSs, which is in good accordance with recent studies [2,5,14] and was already suggested in [7]. Our analysis also often reveals coexisting unstable states associated with MI and breathing CSs that can in practice preclude the observation of stable combs. Care must therefore be taken in interpreting some reported experimental results: they may be associated with rapid fluctuations and only appear stable because of the averaging of spectrum analyzers.

Our next example (Fig. 3) is an octave-spanning comb, strongly influenced by higher-order dispersion. The simulation parameters are radically different and are approximated from the experiment of [15] (see caption). Again, based on the same model Eq. (3), we observe an excellent agreement between the stable steady-state numerical spectrum plotted in Fig. 3(a) and the experimental measurements (see Fig. 2 in [15]). At this point we must emphasize that, despite the large number of spectral modes included (1024), the computation time in obtaining the results shown in both Figs. 2(a) and 3(a) was of the order of seconds on a standard computer. It is precisely this unprecedented speed that is the key advantage of our technique. In fact, to our knowledge, the Kerr comb of Fig. 3(a) has the largest number of optical modes obtained from a theoretical model. Simulating octave-spanning combs with sub-40 GHz repetiton rates would necessitate ramping up the number of modes to 4096. In

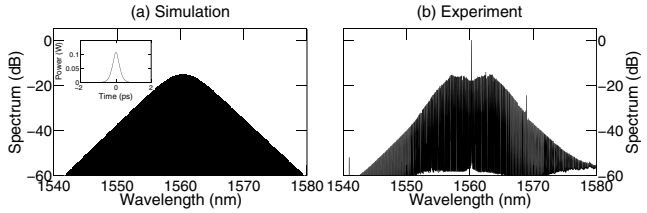

Fig. 2. (a) Steady-state solution of Eq. (3) for a critically coupled, 3.8 mm diameter MgF_2 whispering gallery mode resonator with a 40 μm mode-field diameter and a loaded $Q = 1.90 \cdot 10^9$. FSR = 18.2 GHz; $\gamma = 0.032$ W^{-1} km^{-1}; $\beta_2 = -13$ ps^2 km^{-1}; $\alpha = \theta = 1.75 \cdot 10^{-5}$; $P_{\text{in}} = 55.6$ mW; $L = 11.9$ mm; $\delta_0 = 0.0012$. (b) Corresponding experimental spectrum after [13].

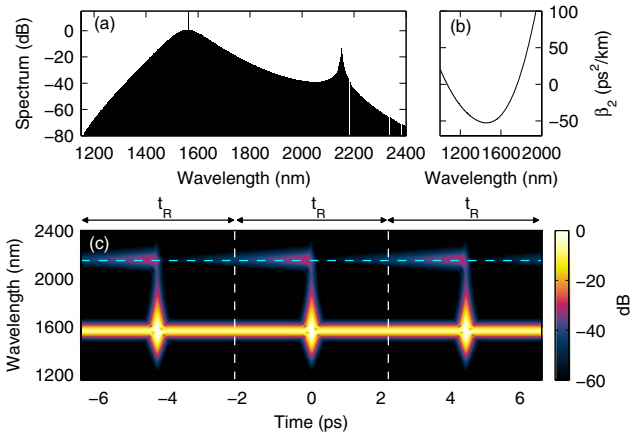

Fig. 3. (Color online) (a) Steady-state solution of Eq. (3) with parameters mimicking a critically coupled, 200 μm diameter silicon nitride resonator with a loaded $Q = 3 \cdot 10^5$ approximated from [15]. Dispersion as per (b); FSR = 226 GHz; $\gamma = 1\ \mathrm{W^{-1}\,m^{-1}}$; $\alpha = \theta = 0.009$; $P_{\mathrm{in}} = 755$ mW; $L = 628$ μm; and $\delta_0 = 0.0534$. (c) Time-frequency representation of the simulation result calculated using a 100 fs gate function. Subsequent roundtrips are separated by vertical lines, whilst the horizontal line indicates the predicted Čerenkov wavelength.

this case, computation time increases to about 2–3 min (or less if considering neighboring solutions), but is still very reasonable.

A particular feature seen in Fig. 3(a) is the strong narrowband low-frequency component centered about 2150 nm. A similar feature can be witnessed in the corresponding experimental measurements [15], and also in other previous experiments (see, e.g., Fig. 1 in [16]). We interpret this component as a Čerenkov-like resonant dispersive wave (DW) emitted by the CS circulating in the resonator [17]. To show this explicitly, we plot in Fig. 3(c) the time-frequency representation of the intracavity electric field. Here we exploit the periodic boundary conditions, and expand the fast temporal axis across three cavity roundtrips. We can clearly see how the intracavity field consists of a train of pulses atop a cw background (i.e., CSs) and we can identify the narrowband 2150 nm component as DWs emitted by individual CSs. This is further highlighted by the dashed horizontal line in Fig. 3(c), which indicates the predicted wavelength λ_{DW} of a Čerenkov wave. Specifically, neglecting the nonlinear contribution, the pertinent phase-matching condition governing the resonant DW is $\beta(\omega_{\mathrm{DW}}) = \beta(\omega_{\mathrm{CS}}) - \beta_1(\omega_{\mathrm{CS}}) \cdot (\omega_{\mathrm{CS}} - \omega_{\mathrm{DW}})$ [17], where $\omega_{\mathrm{DW}} = 2\pi c/\lambda_{\mathrm{DW}}$ and ω_{CS} are the central (angular) frequencies of the DW and the CS, respectively. With our numerical parameters, this condition yields $\lambda_{\mathrm{DW}} = 2149$ nm, in excellent agreement with the observed spectral peak in Fig. 3(a). Because a (cavity) soliton in the anomalous GVD regime can only excite DWs in the normal GVD regime, our observations suggest that the ubiquitous asymmetry of Kerr combs toward the normal GVD regime may in fact be explained by the excitation of resonant DWs by CSs in the anomalous GVD region in a way akin to supercontinuum generation [17]. Finally, we note that DW emission has recently been described in terms of cascaded four-wave mixing, which further highlights its relevance to Kerr combs [18].

In conclusion, we have used a generalized LL equation to model high-Q resonator Kerr frequency combs. It can be solved with a Newton–Raphson solver, providing results in a matter of seconds, much faster than any other technique, and for widely different cases, all the way to octave-spanning combs with hundreds of modes. Our results are in good agreement with experiments, proving that the LL model captures the essential physics of Kerr combs. We also find that Kerr frequency combs are associated in the temporal domain with CSs [7] and associated DWs. CSs are well known localized dissipative structures that have been studied extensively in the past, in particular in the spatial domain [9,10], so we anticipate that the LL model will provide both a deeper understanding of Kerr frequency combs and computational efficiency. The Newton method also provides information about dynamical instabilities of Kerr combs through an eigenvalue analysis of the Jacobian of the system, which is obtained at no extra cost. Some of our preliminary results highlight the presence of Hopf bifurcations associated with breathing CSs, i.e., combs with periodically modulated features.

We thank Dr. I. S. Grudinin for kindly providing experimental data. We also acknowledge support from the Marsden Fund of The Royal Society of New Zealand.

References

1. T. J. Kippenberg, R. Holzwarth, and S. A. Diddams, Science **332**, 555 (2011).
2. F. Ferdous, H. Miao, D. E. Leaird, K. Srinivasan, J. Wang, L. Chen, L. T. Varghese, and A. M. Weiner, Nat. Photonics **5**, 770 (2011).
3. I. H. Agha, Y. Okawachi, and A. L. Gaeta, Opt. Express **17**, 16209 (2009).
4. Y. K. Chembo and N. Yu, Phys. Rev. A **82**, 033801 (2010).
5. A. B. Matsko, A. A. Savchenkov, W. Liang, V. S. Ilchenko, D. Seidel, and L. Maleki, Opt. Lett. **36**, 2845 (2011).
6. L. A. Lugiato and R. Lefever, Phys. Rev. Lett. **58**, 2209 (1987).
7. F. Leo, S. Coen, P. Kockaert, S.-P. Gorza, Ph. Emplit, and M. Haelterman, Nat. Photonics **4**, 471 (2010).
8. M. Haelterman, S. Trillo, and S. Wabnitz, Opt. Commun. **91**, 401 (1992).
9. A. J. Scroggie, W. J. Firth, G. S. McDonald, M. Tlidi, R. Lefever, and L. A. Lugiato, Chaos Solitons & Fractals **4**, 1323 (1994).
10. L. A. Lugiato, IEEE J. Quantum Electron. **39**, 193 (2003).
11. S. Coen and M. Haelterman, Opt. Lett. **24**, 80 (1999).
12. S. Coen and M. Haelterman, Opt. Lett. **26**, 39 (2001).
13. I. S. Grudinin, L. Baumgartel, and N. Yu, Opt. Express **20**, 6604 (2012).
14. A. B. Matsko, A. A. Savchenkov, V. S. Ilchenko, D. Seidel, and L. Maleki, Phys. Rev. A **85**, 023830 (2012).
15. Y. Okawachi, K. Saha, J. S. Levy, Y. H. Wen, M. Lipson, and A. L. Gaeta, Opt. Lett. **36**, 3398 (2011).
16. M. A. Foster, J. S. Levy, O. Kuzucu, K. Saha, M. Lipson, and A. L. Gaeta, Opt. Express **19**, 14233 (2011).
17. J. M. Dudley, G. Genty, and S. Coen, Rev. Mod. Phys. **78**, 1135 (2006).
18. M. Erkintalo, Y. Q. Xu, S. G. Murdoch, J. M. Dudley, and G. Genty, Phys. Rev. Lett. **109**, 223904 (2012).